Available online at www.eccomasproceedia.org
Eccomas Proceedia SMART (2023) 23-34

ECCOMAS
Proceedia

X ECCOMAS Thematic Conference on Smart Structures and Materials
SMART 2023
D.A. Saravanos, A. Benjeddou, N. Chrysochoidis and T. Theodosiou (Eds)

A PROBABILISTIC REDUCED ORDER MODELING FRAMEWORK FOR THE DESIGN OF COMPOSITE SCAFFOLDS IN BONE TISSUE ENGINEERING

GEORGE I. DRAKOULAS*, THEODORE V. GORTSAS*, AND DEMOSTHENES POLYZOS*

* Department of Mechanical Engineering and Aeronautics,
University of Patras, Rion, 26500, Patras, Greece
e-mail: g.drakoulas@upnet.gr, gortsas@upatras.gr, polyzos@mech.upatras.gr

Abstract. In recent years, additive manufacturing has shown great potential for the design of geometrically complex, biocompatible, and biodegradable scaffold-assisted implants in bone tissue engineering. Mechanoregulatory models have shown that the differentiation of the cells on the scaffold is impacted by quantities such as the surface shear stress which appears when the scaffold is mechanically loaded, and the wall shear stress that emerges due to the interaction of the scaffold with the blood flow around it. However, the performance of the scaffold depends on various parameters such as material composition, geometry, loading, and flow conditions. In this work, to gain an understanding of the parameters' impact on the behavior of the scaffold, a four-layer/strut orthogonal scaffold with isometric pores made of polylactic acid and reinforced by 5% stainless steel particles, is numerically studied. The high-fidelity structural analysis is performed with the Boundary Element Method while for the fluid simulations, the element-based Finite Volume Method is employed. The effect of the variability in the material properties and the boundary conditions of the computational models is explored by utilizing probabilistic deep learning-based reduced order models (ROMs) for the structural and fluid problem. Regarding the training of the ROMs, it is shown that a low number of full-scale simulations is required to compute the high-fidelity data. To implement the ROMs, proper orthogonal decomposition is used to compute a low dimensional basis, and a Bayesian neural network to map the simulation parameters to the reduced data as well as to capture the epistemic uncertainties in the regression task. The predicted results demonstrate the ability of the ROMs to provide numerical results with good accuracy for the parameter range of interest.

Keywords: Computational Mechanics, Reduced Order Models, Bone Scaffolds, Additive Manufacturing, Deep Learning, Bayesian Neural Networks.

1 INTRODUCTION

Biodegradable and biocompatible scaffolds used for bone tissue engineering and bone repair in critical-size fractures have recently attracted massive attention. The scaffolds are designed so that their mechanical properties are as similar as possible to those of the

© 2023 The Authors. Published by Eccomas Proceedia.
Peer-review under responsibility of the organizing committee of SMART 2023.
doi: 10.7712/150123.9761.455453

physiological bone, with sufficient porosity to facilitate vascularization, nutrition transport, as well as cell adhesion, and proliferation. Among others, the material properties, the geometry, and the loading conditions are crucial parameters that significantly affect the bone regeneration process. Computational structural mechanics (CSM) and fluid dynamics (CFD) are commonly utilized to replace in vitro and in vivo research, targeting to predict bone regeneration in the environment of a biocompatible scaffold. Various computational models have been implemented to calculate the surface strains in the solid phase as well as the wall shear stresses in the interstitial fluid phase during the differentiation process. Some representative works on the subject are those of [1- 5].

While computational mechanics remains a robust tool to effectively predict scaffold-aided bone healing processes, the simulation cost is rapidly increasing when various high-fidelity models (HFMs) are required to estimate the effect of the model parameters (e.g., material properties, boundary conditions, geometrical parameters, etc.) in the cells' behavior on the scaffold. To decrease the computational time, reduced-order models (ROMs) can be utilized. ROMs as part of a broad category, called surrogate modeling, provide fast solutions with a controlled loss of accuracy [6]. Over the last few years, deep learning (DL) methods have been effectively used in the formulation of non-intrusive ROMs for non-linear, partial differential equations [7]. When dealing with steady-state numerical problems, the reduced basis method has been used to decrease the dimensions of the high-fidelity solutions, stored in a database, called snapshot matrix. To achieve that, the proper orthogonal decomposition is commonly employed using the singular value decomposition (SVD) technique, to identify a linear basis, and project the snapshot matrix in a low dimensional subspace. As a second step, a DL-based regression model is obtained to map the parameter values used to define the HFMs, to the projected data [8].

In this work, a rectangular and four-layer/strut orthogonal scaffold with isometric pores made by polylactic acid PLA/316L with 5% stainless steel particle content, is numerically studied. The objective is to develop two DL-ROMs and estimate the effect of the material properties, the structural loading, and the fluid flow conditions on the distribution of the surface strains and the wall shear stresses on the scaffold surface. To accomplish that the Boundary Element Method (BEM) [9] is used to solve the Navier-Cauchy equation, while the element-based Finite Volume Method (EbFVM) [10] is employed to solve the Navier Stokes equations. The developed DL-ROM includes a state-of-the-art dimensionality reduction technique based on SVD update to compute the basis vector incrementally, during the simulation process [6]. To account for the uncertainties in the regression model parameters, caused by the limited HFM simulations, we are dealing with, a Bayesian model can be employed; see e.g Gaussian processes [11, 12] or Bayesian neural networks (BNNs) [13, 14] to list a few. In the present work, a probabilistic DL model is employed. In particular, a BNN is utilized to map the parameter vectors to the extracted linearly projected data. BNNs, as part of the probabilistic machine learning, allow for the calculations of the epistemic uncertainties, related to the weights of the artificial neural networks (ANNs), avoiding the limitations of the deterministic models by providing the confidence of intervals in the ROM predictions [15].

2 PROBLEM FORMULATION

In this section, the scaffold geometry, the material properties, and the numerical models for the high-fidelity structural and the CFD analysis via the BEM and the EbFVM, respectively, are briefly described.

A four-layer/strut orthogonal scaffold geometry is examined, composed of 8 filament rows in a 0°/90° stacking sequence (Fig. 1) and with a porosity that reaches 65%. The scaffold is made of PLA reinforced by a 5 % stainless steel particle content (PLA/316L). PLA is commonly utilized for bone tissue engineering due to its high biocompatibility and suitable biodegradation, demonstrating an elastic modulus close to the natural bone [1]. Furthermore, the addition of stainless steel particles enhances flexural, compressive modulus, and fatigue resistance [3]. In the present work, we assume that the composite material is isotropic and linear elastic with Young modulus E = 0.28 GPa and Poisson ratio ν = 0.37.

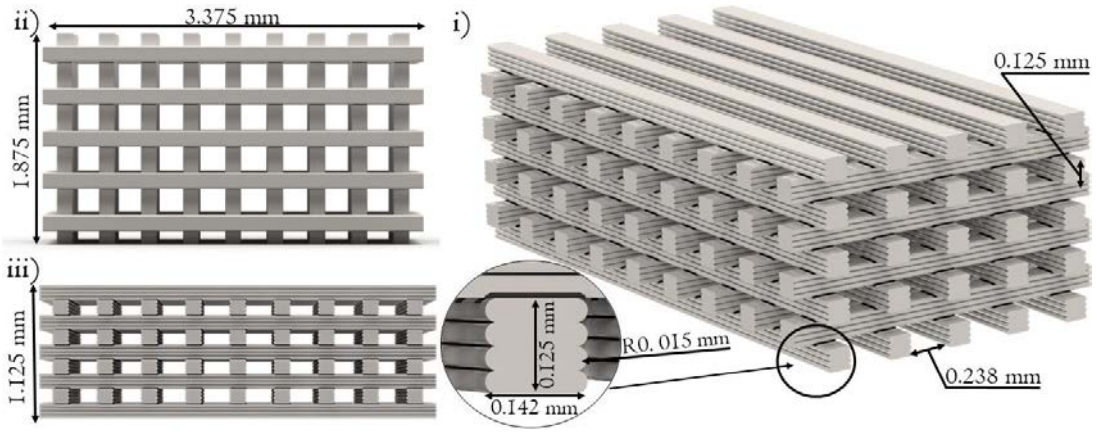

Figure 1: Geometric representation of the rectangular and four-layer scaffold. The geometric details of the designed scaffold are indicated in i) isometric, ii) upper side, and iii) left side view

To evaluate the structural behavior of the scaffold when loaded with a bending load, and provide the strain distribution on the scaffold surface, the Navier-Cauchy equations are solved using the BEM, which is a robust and efficient tool for solving linear elastic problems [9,16-17]. The main advantage of the BEM is that for the application of the method only the boundary needs to be discretized. The equilibrium equation for an isotropic and homogeneous linear elastic body is the well-known Navier-Cauchy equation accompanied by proper boundary conditions.

An integral representation of the solution to the elastic problem can be provided via the fundamental solution $U_{ij}^{*}(\mathbf{x},\mathbf{y})$ of the Navier-Cauchy equation as follows [9]:

$$C_{ij}(\mathbf{x})u_j(\mathbf{x})+\int_S T_{ij}^{*}(\mathbf{x},\mathbf{y})u_j(\mathbf{y})dS_{\mathbf{y}}=\int_S U_{ij}^{*}(\mathbf{x},\mathbf{y})t_j(\mathbf{y})dS_{\mathbf{y}} \tag{1}$$

where $u_i(\mathbf{x})$ stand for the Cartesian components of the displacement vector at the field point $\mathbf{x}$ of the elastic body with volume Ω and external boundary S, $t_i(\mathbf{x})$ represents the components of traction vector defined at the boundary S, $\mathbf{y}$ denotes the source point, $T_{ij}^{*}(\mathbf{x},\mathbf{y})$ is the traction

field corresponding to the fundamental solution $U_{ij}^{*}(\mathbf{x},\mathbf{y})$, $C_{ij}(\mathbf{y})$ is the jump tensor obtaining the values $C_{ij}(\mathbf{y})=\delta_{ij}$ when $\mathbf{y}\in\Omega$, and $C_{ij}(\mathbf{y})=\delta_{ij}/2$ when $\mathbf{y}$ belongs to a smooth part of the boundary S, and δ_{ij} is the Kronecker delta.

Assuming that the boundary of the body is discretized into boundary elements, with each element defined by a specific number of nodes, collocating Eq. (1) to each node of the boundary and considering the boundary conditions of the problem a linear system of equations $\mathbf{A}\cdot\mathbf{x}=\mathbf{b}$ is obtained, where the matrix $\mathbf{A}$ is dense and non-symmetric and the vector $\mathbf{x}$ contains the unknown displacements and tractions for the nodes of the boundary.

After the computation of the displacement and traction vectors for all the nodes of the boundary, in a post-processing step, the strain can be calculated for a point lying in a smooth part of the boundary as follows, [9],

$$\frac{1}{2}\partial_k u_i(\mathbf{x})+\int_{\partial\Omega} P_{kij}^{*}(\mathbf{x},\mathbf{y})u_j(\mathbf{y})dS_{\mathbf{y}}=\int_{\partial\Omega} Q_{kij}^{*}(\mathbf{x},\mathbf{y})t_j(\mathbf{y})dS_{\mathbf{y}} \tag{2}$$

where the expressions for the tensor kernels $P_{kij}^{*}(\mathbf{x},\mathbf{y})$ and $Q_{kij}^{*}(\mathbf{x},\mathbf{y})$ can be found in [9].

For the solution of the problem with the BEM, an in-house developed C++ software is employed, using fast solvers for integral equations based on Hierarchical Matrices and algebraic compression techniques such as the Adaptive Cross Approximation [18, 19].

In a second step, we examine the interaction of the scaffold with the interstitial fluid flow. The objective is to compute the distribution of the wall shear stress on the scaffold surface, as this quantity is often linked to the differentiation of the cells on the scaffold. To this end, CFD simulations using the EbFVM are performed to solve the nonlinear Navier-Stokes equations for the Newtonian fluid with density $\rho = 1000\ kg/m^3$ and dynamic viscosity $\mu = 0.001$ Pa·s (Fig.2).

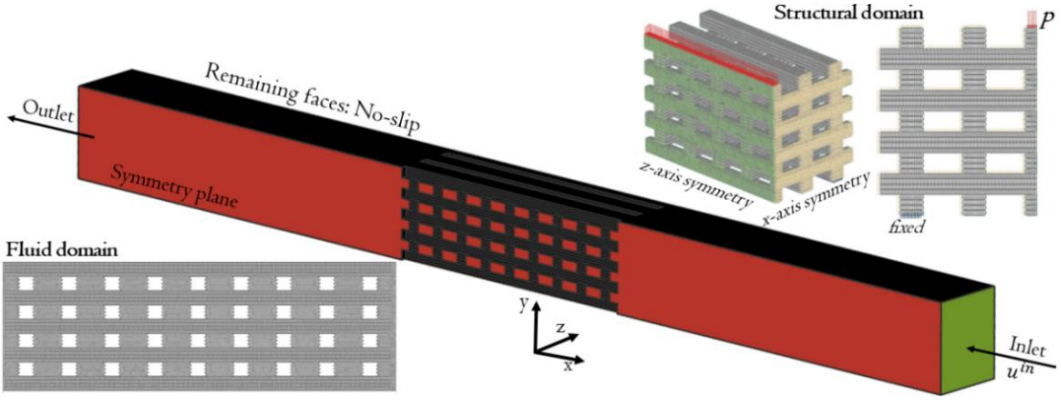

Figure 2. Mesh grid and boundary conditions for the CFD and CSM simulations.

3 REDUCED ORDER MODELING USING BAYESIAN DEEP LEARNING

In this section, the techniques utilized to construct the DL-based ROM are presented. The linear dimensionality reduction procedure as well as the integration with the BNN used for the parameter regression are described.

Consider a parametric vector field $\boldsymbol{\upsilon}(\mathbf{x};\boldsymbol{\varphi}):\Omega\, x\, \mathbb{R}^{\xi}\rightarrow\mathbb{R}^{3}$ corresponding to an unknown primary or derived field of interest for a boundary value problem described by either the Navier-Cauchy or the steady state Navier Stokes equations, where $\boldsymbol{\varphi}$ is a parameter vector and $\mathbf{x}\in\Omega$ denotes a point of the domain Ω or its boundary. The vector $\boldsymbol{\varphi}$ is sampled from a closed and bounded parameter space $P\subset\mathbb{R}^{\xi}$, where ξ is the dimension of the parameter vector.

The spatially discretized form of the parametrized HFM solution can be represented as, $\boldsymbol{\upsilon}_h(\boldsymbol{\varphi})$, $\boldsymbol{\upsilon}_h:\mathbb{R}^{\xi}\rightarrow\mathbb{R}^{N_h}$, where $h>0$ denote a discretization parameter and N_h is the dimension of the discretized function $\boldsymbol{\upsilon}$. To construct the ROM, the Latin hypercube sampling methodology is utilized to uniformly sample the parameters from the space *P*, and split them into two sets; $\varphi^{tr}=\{\boldsymbol{\varphi}_1^{tr},...,\boldsymbol{\varphi}_m^{tr}\}$ and $\varphi^{te}=\{\boldsymbol{\varphi}_1^{te},...,\boldsymbol{\varphi}_n^{te}\}$ corresponding to the *m* training and *n* testing parameter vectors. The snapshot matrix $S_h\in\mathbb{R}^{N_h\,x\,m}$ using the φ^{tr}, is formed as follows,

$$\mathbf{S}_h=[|\,\boldsymbol{\upsilon}_h(\boldsymbol{\varphi}_1^{tr})\,|...|\,\boldsymbol{\upsilon}_h(\boldsymbol{\varphi}_m^{tr})\,|] \tag{3}$$

A state-of-the-art truncated SVD update methodology [6] is employed to generate a reduced basis for the snapshot matrix (Eq. 3). The utilized methodology can efficiently compress large snapshot matrices to generate a unique linear basis $\mathbf{U}$, incrementally. Given the snapshot matrix containing the solutions for all the parameters (Eq. 3), the low-dimensional data for a single parameter vector $\boldsymbol{\varphi}_j^{tr}$ is obtained as follows,

$$\boldsymbol{\upsilon}_n(\boldsymbol{\varphi}_j^{tr})=\mathbf{U}^T\boldsymbol{\upsilon}_h(\boldsymbol{\varphi}_j^{tr}) \tag{4}$$

where *n* is the rank of the basis matrix $\mathbf{U}$, and the size of the projected solution $\boldsymbol{\upsilon}_n(\boldsymbol{\varphi}_j^{tr})$.

3.1 Bayesian neural networks for parameter regression

One of the main objectives of this work is to develop a ROM framework to decrease the computational cost related to the simulation time of data generation. Since only a limited amount of high-fidelity solutions are to be used for the ROM construction, a probabilistic machine-learning model is formulated to quantify the uncertainties introduced in the regression task. In particular, we employ a BNN to provide useful insight into the regions that include high uncertainty predictions, and further HFMs are required to enrich the ROM performance [20]. In general, BNNs can model the data uncertainty also called *aleatoric* and the model uncertainty, known as *epistemic* [21]. Aleatoric uncertainty refers to the randomness inherited in the observations, while epistemic uncertainty is derived from the model parameters, caused by insufficient data. In this work, BNNs are utilized to account for the epistemic uncertainties related to the effect of the low number of HFMs used to develop the DL-ROM.

BNNs are a combination of statistical models and artificial neural networks (ANN) [22]. They provide the ability to combine prior and likelihood aiming to implement probabilistic predictions by assigning distributions over the NN parameters (weights and biases). BNNs can estimate the confidence interval of the predictions, by providing as output a mean value and a raw variance, allowing for better generalization, compared to ordinary ANNs. The epistemic

uncertainty of the BNN is calculated by assigning distribution over the ANN parameters.

Once the basis of the snapshot matrix is derived, and the projected solutions have been calculated, a DL-based regression model is employed to map the input parameters $\boldsymbol{\varphi}_j^{tr}$ to the linearly projected data $\boldsymbol{\upsilon}_n(\boldsymbol{\varphi}_j^{tr}),\quad j=1,...,m.$ The regression step is performed during the offline phase using the labeled training dataset $D=\{(\boldsymbol{\varphi}_j^{tr},\boldsymbol{\upsilon}_n(\boldsymbol{\varphi}_j^{tr})):i=1,..,m\}$.

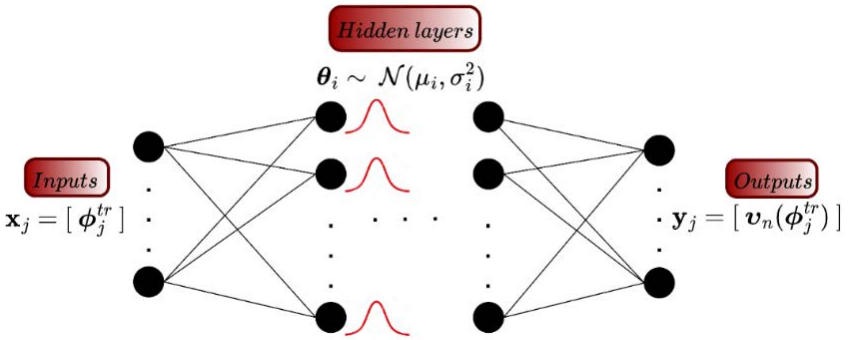

Figure 3. The architecture of the Bayesian neural network (BNN), as part of the ROM framework.

In particular, given the training labeled dataset D, composed of the sets $\mathbf{x}=\{\boldsymbol{\varphi}_1^{tr},...,\boldsymbol{\varphi}_m^{tr}\}$ and $\mathbf{y}=\{\boldsymbol{\upsilon}_n(\boldsymbol{\varphi}_1^{tr}),...,\boldsymbol{\upsilon}_n(\boldsymbol{\varphi}_m^{tr})\},$ Bayesian inference [23] aims to compute the posterior distribution over the weights $p(\boldsymbol{\omega}\,|\,D)$ of the model $\boldsymbol{\omega}$, according to Bayes' rule,

$$p(\boldsymbol{\omega}\,|\,D)=\frac{p(D\,|\,\boldsymbol{\omega})\,p(\boldsymbol{\omega})}{p(D)} \tag{5}$$

where $p(\boldsymbol{\omega})$ is the prior belief on the probability density of the model parameters, $p(D)$ is the marginal probability with $p(D)=\int_{\boldsymbol{\omega}} p(D,\boldsymbol{\omega})p(\boldsymbol{\omega})d\boldsymbol{\omega}$, and $p(\mathbf{y}\,|\,\mathbf{x},\boldsymbol{\omega})$ is the model likelihood. Therefore, the prediction for a testing parameter $\boldsymbol{\varphi}_j^{te}$ is derived by computing the posterior predictive distribution, written as,

$$p(\boldsymbol{\upsilon}_n(\boldsymbol{\varphi}_j^{te})\,|\,\boldsymbol{\varphi}_j^{te},\mathbf{D})=\int p(\boldsymbol{\upsilon}_n(\boldsymbol{\varphi}_j^{te})\,|\,\boldsymbol{\varphi}_j^{te},\boldsymbol{\omega})p(\boldsymbol{\omega}\,|\,D) \tag{6}$$

However, the evaluation of the likelihood function $p(D\,|\,\boldsymbol{\omega})$ and the marginal probability $p(D)$ is often analytically intractable or even computationally prohibitive [24]. Hence, variational inference [25] is utilized to approximate the true posterior $p(\boldsymbol{\omega}\,|\,D)$, using a surrogate model representing a distribution function $q(\boldsymbol{\omega}\,|\,\boldsymbol{\theta})$, with parameters $\boldsymbol{\theta}$.

In this work, BNNs are employed to estimate the distribution $q(\boldsymbol{\omega}\,|\,\boldsymbol{\theta})$. BNNs utilize an ANN architecture to approximate the functional relationship of the labeled dataset D, in a probabilistic manner. Specifically, an ANN is composed of an arbitrary number of neurons and layers, that define a mathematical function consisting of affine transformations, followed by a

non-linear activation function. The non-linear mapping $f:\mathbb{R}^{\xi}\rightarrow\mathbb{R}^{n}$ for a training parameter set $\boldsymbol{\varphi}_j^{te}$ can be expressed as,

$$\tilde{\boldsymbol{\upsilon}}_n(\boldsymbol{\varphi}_j^{te}) = f(\boldsymbol{\upsilon}_n(\boldsymbol{\varphi}_j^{te}); \mathbf{w}_f, \mathbf{b}_f) \tag{7}$$

where $\mathbf{w}_f, \mathbf{b}_f$ are the vectors containing the ANN weight and bias parameters.

In the context of BNNs, prior distributions $p(\boldsymbol{\omega}),$ are assigned to the ANN parameters, instead of considering only a single set. Gaussian distributions are often used to define the variational posterior of the ANN parameters distributions, $\boldsymbol{\theta}_i = N \sim (\mu_i, \sigma_i^2)$ where μ_i is the mean and σ_i is the variance of the distribution at a specific neuron of a layer (Fig. 3). To identify the optimum BNN parameters $\boldsymbol{\theta} = (\boldsymbol{\mu}, \boldsymbol{\sigma})$ and ensure that the posterior $q(\boldsymbol{\omega}\,|\,\boldsymbol{\theta})$ can approximate the posterior $p(\boldsymbol{\omega}\,|\,D),$ the Kullback-Leibler divergence D_{KL} is utilized [21].

In particular, the KL objective for posterior inference given the data is to utilize a backpropagation algorithm and minimize the following loss function,

$$F(D,\boldsymbol{\theta}) = D_{KL}(q(\boldsymbol{\omega}\,|\,\theta)\,||\,p(\boldsymbol{\omega}) - \mathrm{E}_{q(\boldsymbol{\omega}|\boldsymbol{\theta})}\log p(D\,|\,\boldsymbol{\omega}) \tag{8}$$

where the first term is the KL divergence between the variational distribution $q(\boldsymbol{\omega}\,|\,\boldsymbol{\theta})$ and the prior $p(\boldsymbol{\omega})$ and is called the complexity loss, while the second term is the expected value of the likelihood with respect to the variational distribution, referred to as the likelihood cost.

4. NUMERICAL RESULTS

In this section, a comparison between the probabilistic ROM results and the HFM solutions is presented to validate the accuracy of the ROMs and provide the solutions for the CSM and CFD simulations. The accuracy of the predictions is examined using the normalized root mean squared (nrms) error, ε_{nrms}. The DL models are implemented in TensorFlow Probability 0.19.0 using an Intel Core i7 @ 2.20GHz, NVIDIA Ge-Force GTX 1050 Ti GPU computer.

To reduce the computational time of the structural simulations while preserving accuracy, one-quarter of the scaffold geometry is utilized for the numerical analysis and the construction of the database for the ROM employment. In particular, symmetry conditions are defined both in the *x*- and *z-axis* (Fig. 2). A vertical compressive load with magnitude *p* is imposed on the upper, central face of the symmetrical scaffold, while the bottom left face is kept fixed, aiming to simulate a three-point bending loading scenario. The surface mesh grid consists of 252,720 isoparametric, linear, quadrilateral elements, resulting in 252,550 nodes. The mean element size is equal to 0.01mm, derived after a mesh convergence analysis.

For the fluid simulations, the laminar inlet flow is perpendicular to the top plane of the scaffold, and the symmetry wall is defined on the *z-axis* to decrease the simulation time. No-slip condition (zero velocity) is used on the boundary wall surface area and zero pressure on the outlet face (Fig. 2). The commercial software Simcenter 3D Multiphysics solver is employed to simulate the HFMs using the EbFVM. A fine mesh grid has been formulated, including 26,219,072 tetrahedral solid elements, resulting in 4,620,051 nodes.

4.1 ROM results for the CSM simulation

The first DL-based ROM is employed to provide the surface strains of the CSM simulation on the scaffolds for a given parameter vector composed of the material properties and the pressure load. In particular, the young modulus (E), the Poisson ratio (v), and the pressure load (p), $E_i \in [0.2, 2]\ GPa$, $v_i \in [0.3, 0.4]$, *and* $p_i \in [1, 10]\ MPa$, respectively, define the parameter vector, $\boldsymbol{\varphi}_j = [E_j, v_j, p_j]$. The Navier-Cauchy equations are solved for 40 parameters to construct the database for the DL-ROM training, where 36 parameters are used for training and 4 to test the developed ROM. The developed probabilistic ROM framework is implemented to reconstruct the surface strain distribution γ_{srf} on the scaffold surface, obtained with the BEM (Ch. 2) using the following equation,

$$\gamma_{srf} = \frac{1}{2}(\varepsilon_1 - \varepsilon_2) \tag{9}$$

where ε_1 and ε_2 are the principal strains on the element face on the surface of the scaffold. The scaffold surface is the region of interest, composed of 252,720 nodes. Each HFM solution requires 15 mins, while for the generation of the snapshot matrix, 9 hrs are needed.

Regarding the dimensionality reduction of the generated dataset, we apply the truncated SVD update methodology [6], for every four HFM solutions, with a truncation error $\varepsilon = 5x10^{-5}$. We keep then one basis vector from the resulted basis matrix, capturing the 99 % of the singular values cumulative percentage. Then, data standardization is applied to the linearly projected training solutions, before they are passed to the BNN aiming to employ the probabilistic regression task. As concerns the BNN architecture, a Gaussian distribution with zero mean and variance equal to one is obtained as a prior for the ANN parameters. One dense variational layer is employed, with 6 neurons and the leaky relu activation function, followed by a second linear dense variational layer. The BNN is trained for 30,000 epochs, with a learning rate of 0.001, using the Adam optimizer.

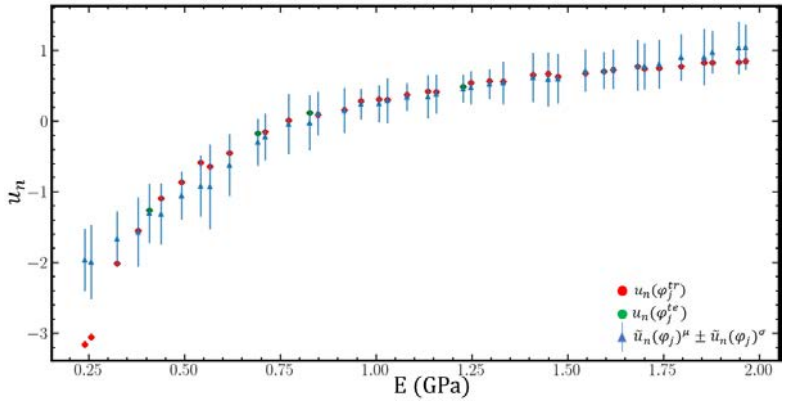

Figure 4. Reference linear projected data for both training [$\boldsymbol{u}_n(\boldsymbol{\varphi}_j^{tr})$] and testing [$\boldsymbol{u}_n(\boldsymbol{\varphi}_j^{te})$] parameters, as well as the mean (μ) and standard deviation (σ) predictions [$\tilde{\boldsymbol{u}}_n(\boldsymbol{\varphi}_j)^{\mu} \pm \tilde{\boldsymbol{u}}_n(\boldsymbol{\varphi}_j)^{\sigma}$], across Young's modulus.

Once the BNN is trained, the model is evaluated $N_E = 100$ times for each parameter vector to generate the standard deviation and the mean predicted quantities. To get a clear insight into

the BNN predictions, in Fig. 4, we present the BNN predictions of the linear projected across the Young's modulus. It is observed that the BNN presents the most uncertain predictions for the lower inlet velocities, which further do not include the reference projected solutions in the confidence interval. This indicates that more simulations are required in this region, to enrich both the basis vector and the BNN training. As concerns the other parameters, the mean predicted values are close to the reference data, obtaining low standard deviation values.

In Fig. 5, we plot the high-fidelity BEM solution and the mean prediction of the ROM for the parameter $\boldsymbol{\varphi}_2^{te} = [9.6, 0.32, 5.25]$. It is shown that the mean ROM prediction is close to the BEM solution, providing smooth results on the scaffold surface. To further access the accuracy of the proposed probabilistic ROM framework, we calculate the nrms error ε_{nrms} for the parameter $\boldsymbol{\varphi}_2^{te}$, which is equal to 0.001.

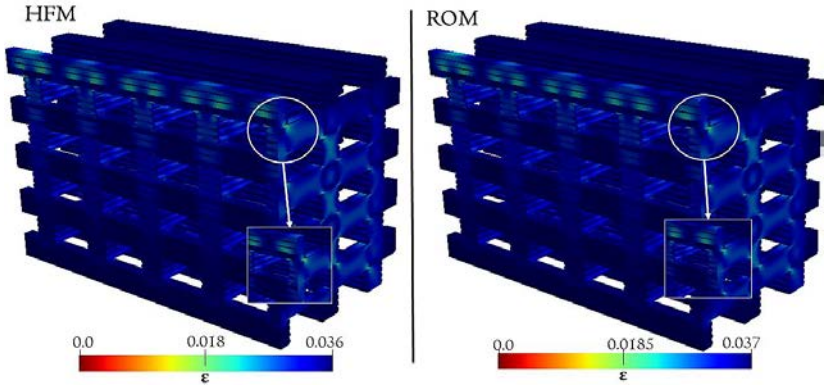

Figure 5. Comparison between the HFM solution to the mean ROM prediction of the surface strain distribution on the scaffold for the testing parameter $\boldsymbol{\varphi}_2^{te} = [9.6, 0.32, 5.25]$.

4.2 ROM results for the CFD simulation

As a second step, an additional DL-ROM is employed to compute the generated wall shear stresses imposed by the fluid flow on the surface of the scaffold for the various inlet velocities. The inlet velocity $v^{in} \in [1,10]\ mm/s$, is used to define the parameter vector $\boldsymbol{\varphi}_j = [u_j^{in}]$. The developed ROM aims to provide the wall shear stress distribution on the scaffold surface for a given inlet velocity. The Navier-Stokes equations are solved for 12 parameters, where 10 parameters are used for training and 2 for testing (Ch. 2). The HFM solution requires 30 mins for each parameter, while for the generation of the entire snapshot matrix, 5 hrs are needed. The area of interest defined on the scaffold surface of the fluid domain includes 1,057,779 nodes.

For the formulation of the DL-ROM, a similar approach as the one presented in Section 4.1 is performed. In particular, a truncation error $\varepsilon = 5x10^{-5}$ is defined for the application of the SVD update, and then one basis vector is utilized, capturing the 98 % of the singular values cumulative percentage. Regarding the BNN, one dense variational layer is obtained, with three neurons using the leaky relu activation function, followed by a second linear dense variational layer with one neuron. We train the BNN for 10,000 epochs, with a learning rate of 0.001.

In Fig. 6, the reference linear projected solutions extracted from the SVD for the training and testing parameters, as well as the mean and the standard deviation of the predicted solutions

using the BNN for each inlet velocity are presented. It is shown that the most uncertainty values are obtained for the higher and lower values of the inlet velocities. The mean predicted solutions are close to reference linear projected data points, both for the training and testing parameters.

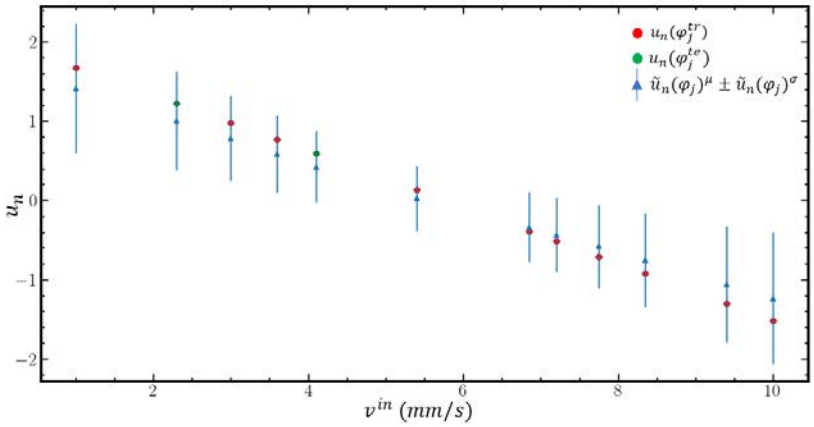

Figure 6. Reference linear projected data for both training $[\boldsymbol{u}_n(\boldsymbol{\varphi}_j^{tr})]$ and testing $[\boldsymbol{u}_n(\boldsymbol{\varphi}_j^{te})]$ parameters, as well as the mean and standard deviation prediction $[\tilde{\boldsymbol{u}}_n(\boldsymbol{\varphi}_j)^{\mu} \pm \tilde{\boldsymbol{u}}_n(\boldsymbol{\varphi}_j)^{\sigma}]$, using the BNN across the velocities.

Then, in Fig 7 we present the HFM and the mean predicted solution for the parameter $\boldsymbol{\varphi}_1^{te} = [9.4]\ mm/s$. It is observed that the developed DL-ROM can predict with good accuracy the wall shear stress on the scaffold domain, in a limited amount of time. In particular, the nrms error ε_{nrms} is equal to 0.03.

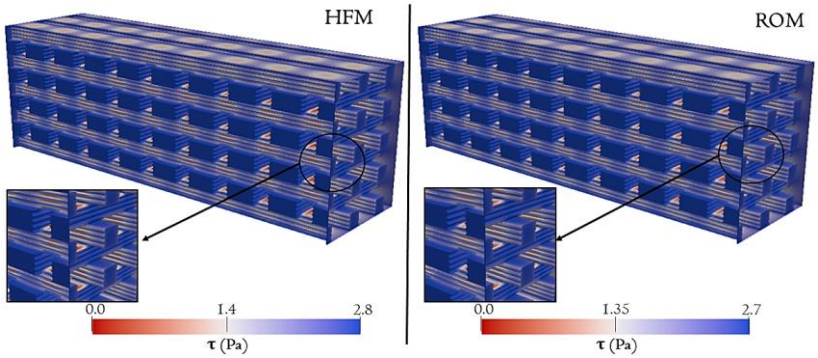

Figure 7. Comparison between the HFM solution to the mean ROM prediction of the wall shear stress distribution on the scaffold surface for the testing parameter $\boldsymbol{\varphi}_1^{te} = [9.4]\ mm/s$.

5 CONCLUSIONS

In this work, a DL-based ROM is implemented to provide the surface strains and the wall shear stresses on an orthogonal scaffold geometry, composed of four-layer struts in a 0°/90° stacking sequence. The scaffold is made of PLA, with 5 % stainless steel particle content. The BEM and the EbFVM are utilized to construct the CSM and CFD simulation data, aiming to employ a DL-ROM that provides the solutions in a limited amount of time. A state-of-the-art SVD method is used to identify a linear basis during the simulation process. To quantify the uncertainties in the model parameters when dealing with a limited dataset, a probabilistic DL-

ROM using BNNs is formulated. It is shown that, for the implementaion of the DL-ROMs, a low number of HFMs is required. Regarding the structural mechanics simulation, the BEM appears to be an ideal methodology to calculate the surface strains, for various material properties and bending pressure loads, providing smooth results on the scaffold surface. Moreover, the developed probabilistic DL-ROM can efficiently predict the surface strains, while the BNN presents higher epistemic uncertainties for the lower parameter values. As concerns the computational fluid dynamics simulation, the ROM can predict with great accuracy the wall shear stress distribution on the scaffold surface, while the BNN shows higher values of uncertainties at the lower and upper extremities of the inlet velocities.

ACKNOWLEDGMENTS

This work is supported by the Hellenic Foundation for Research and Innovation (HFRI) under the "First Call for HFRI. Research Projects to support Faculty members and Researchers and the procurement of high-cost research equipment grant" (Project Number: 2060).

REFERENCES

[1] R. Baptista, M. Guedes, "Morphological and mechanical characterization of 3D printed PLA scaffolds with controlled porosity for trabecular bone tissue replacement," *Materials Science and Engineering: C*, vol. 118, 111528, 2021.

[2] Yin, S., Zhang, W., Zhang, Z., Jiang, X.: Recent Advances in Scaffold Design and Material for Vascularized Tissue-Engineered Bone Regeneration. *Adv. Healthcare Mater*. 8, 1801433, 2019.

[3] N. Cubo-Mateo, L. M. Rodríguez-Lorenzo, "Design of Thermoplastic 3D-Printed Scaffolds for Bone Tissue Engineering: Influence of Parameters of "Hidden" Importance in the Physical Properties of Scaffolds," *Polymers*, vol. 12(7), 1546, 2020.

[4] D. Jiang, F. Ning, Y. Wang, "Additive manufacturing of biodegradable iron-based particle reinforced polylactic acid composite scaffolds for tissue engineering," *Journal of Materials Processing Technology*, vol. 289, 116952, 2021.

[5] W.J. Hendrikson, A.J. Deegan, Y. Yang, C.A. van Blitterswijk, N. Verdonschot, L. Moroni, J. Rouwkema, "Influence of Additive Manufactured Scaffold Architecture on the Distribution of Surface Strains and Fluid Flow Shear Stresses and Expected Osteochondral Cell Differentiation," *Frontiers in Bioengineering and Biotechnology*, vol. 5:6, 2017.

[6] G.I. Drakoulas, T.V. Gortsas, G.C. Bourantas, V.N. Burganos, D. Polyzos, "*FastSVD-ML-ROM*: A reduced-order modeling framework based on machine learning for real-time applications," arXiv preprint arXiv:2207.11842, 2022.

[7] P. Jacquier, A. Abdedou, V. Delmas, A. Soulaimani, "Non-intrusive reduced-order modeling using uncertainty-aware Deep Neural Networks and Proper Orthogonal Decomposition: Application to flood modeling," *Journal of Computational Physics*, vol. 424, 109854, 2021.

[8] G. Mengwu, J.S. Hesthaven, " Reduced order modeling for nonlinear structural analysis using Gaussian process regression," *Comput. Methods Appl. Mech. Engrg*., vol. 341, pp. 807-826, 2018.

[9] D. Polyzos, S.V. Tsinopoulos, D.E. Beskos, "Static and dynamic boundary element analysis in incompressible linear elasticity," *European Journal of Mechanics – A/Solids*, vol. 17, pp. 515–536, 1998.

[10] H.T. Honorio, C.R. Maliska, M. Ferronato, C. Janna, " A stabilized element-based finite volume method for poroelastic problems," *Journal of Computational Physics*, vol. 364, pp. 49-72, 2018.
[11] Williams, Christopher KI, and Carl Edward Rasmussen. *Gaussian processes for machine learning*. Vol. 2, no. 3. Cambridge, MA: MIT press, 2006.
[12] Polyzos KD, Lu Q, Giannakis GB. Ensemble Gaussian processes for online learning over graphs with adaptivity and scalability. IEEE Transactions on Signal Processing. 2021 Oct 26;70:17-30.
[13] R. Maulik, R. Egele, K. Raghavan, P. Balaprakash, "Quantifying uncertainty for deep learning based forecasting and flow-reconstruction using neural architecture ensembles," arXiv preprint: arXiv: 2302.09748v1, 2023.
[14] P. Jacquier, A. Abdedou, V. Delmas, A. Soulaimani, "Non-intrusive reduced-order modeling using uncertainty-aware Deep Neural Networks and Proper Orthogonal Decomposition: Application to flood modeling," *Journal of Computational Physics*, vol. 424, 109854, 2021.
[15] N.E. Silionis, T. Liangou, K.N. Anyfantis, "Conditional Deep generative models as surrogates for spatial field solution reconstruction with quantified uncertainty in Structural Health Monitoring applications," arXiv preprint: arXiv:2302.08329v1, 2023.
[16] D. Rodopoulos, T.V. Gortsas, S.V. Tsinopoulos, D. Polyzos, "Numerical evaluation of strain gradients in classical elasticity through the Boundary Element Method," *European Journal of Mechanics / A Solids*, vol. 86, 104178, 2021.
[17] T.V. Gortsas, S.V. Tsinopoulos, E. Polyzos, L. Pyl, D.I. Fotiadis, D. Polyzos, "BEM evaluation of surface octahedral strains and internal strain gradients in 3D-printed scaffolds used for bone tissue regeneration," *Journal of the Mechanical Behavior of Biomedical Materials*, vol. 125, 104919, 2022.
[18] T.V. Gortsas, S.V. Tsinopoulos, D. Polyzos, "An advanced ACA/BEM for solving 2D large-scale problems with multi-connected domains," *CMES-Computer Modeling in Engineering & Science,* vol. 107(4), pp. 321–343, 2015.
[19] T.V. Gortsas, S.V. Tsinopoulos, D. Polyzos, "An accelerated boundary element method via cross approximation of integral kernels for large-scale cathodic protection problems,", *Computer-Aided Civil and Infrastructure Engineering*, vol 37(7), pp. 848–863, 2022.
[20] A. Olivier, M.D. Shields, L. Graham-Brady, "Bayesian neural networks for uncertainty quantification in data-driven materials modeling," *Comput. Methods Appl. Mech. Engrg*., vol. 386, 114079, 2021.
[21] L.V. Jospin, W. Buntine, F. Boussaid, H. Laga, M. Bennamoun, "Hands-on Bayesian neural networks–a tutorial for deep learning users," arXiv preprint arXiv:2007.06823, 2020.
[22] M. Abdar, F. Pourpanah, S. Hussain, D. Rezazadegan, L. Liu, M. Ghavamzadeh, P. Fieguth, X. Cao, A. Khosravi, U.R. Acharya, V. Makarenkov, S. Nahavandi, "A review of uncertainty quantification in deep learning: techniques, applications and challenges," arXiv:2011.06225, 2021.
[23] G. E.P. Box, G.C. Tiao, "Bayesian inference in statistical análisis," *John Wiley & Sons*, 2011.
[24] Z. Pan, P. Mishra, "Backdoor Attacks on Bayesian Neural Networks using Reverse Distribution," arXiv preprint 2205.09167v1, 2022.
[25] D.M. Blei, A. Kucukelbir, J.D. McAuliffe, "Variational inference: A review for statisticians," *J. Am. Stat. Assoc.*, vol. 112 (518), pp. 859–877, 2017.